

Article citation info:

Zębala W, Młynarski S, Ślusarczyk Ł, Testing and modeling the possibility of using a lamellar grinding wheel with an adaptive background structure, *Eksploracja i Niezawodność – Maintenance and Reliability* 2024; 26(2) <http://doi.org/10.17531/ein/183318>

Testing and modeling the possibility of using a lamellar grinding wheel with an adaptive background structure

Indexed by:



Wojciech Zębala^a, Stanisław Młynarski^a, Łukasz Ślusarczyk^{a,*}

^a Cracow University of Technology, Poland

Highlights

- An innovative abrasive wheel background.
- The concept of a mathematical model to verify various material and construction solutions of abrasive wheel background.
- The research stand was designed to measure the temperature in the grinding zone without direct contact.

Abstract

In the article, the authors present the concept of a mathematical model used to study the influence of the properties of the base materials used to produce an innovative abrasive wheel background on the operating characteristics of the final tool. This model will be used to verify various material and construction solutions. The article also covers the outcomes of research that confirm the developed model's effectiveness in relation to the operation of lamellar grinding discs, as per their intended technological goal. The experiments involved surface grinding with grinding wheels constructed on chosen backgrounds. A dedicated research stand was designed to measure the temperature in the grinding zone without direct contact, using both new and used grinding discs. The tests incorporated various load levels applied by the grinding disc on the workpiece, as well as different working angles of the grinding disc.

Keywords

background of multi-element discs, abrasive discs, mathematical model, temperature, cutting zone.

This is an open access article under the CC BY license (<https://creativecommons.org/licenses/by/4.0/>)

1. Introduction

The purpose of the proper use of the grinding wheel is maintenance its full suitability for grinding the surface of parts in accordance with the technological purpose [1,10]. An important aspect is also the grinding wheel self-regeneration during the process of its use [12,18]. Operational practice indicates the assessment of the technical condition based on the analysis of numerical values of the control parameters [6,23]. The tool wear process can be characterized by the change of control parameters [26,28]. Tool condition monitoring reduces the production costs and time required to service cutting tools as well as increases the efficiency of the manufacturing process [4,5,11]. Various strategies and

techniques are used in the interpretation of measured data [20,29,30]. Control actions are specified based on the obtained data in order to close the process control loop [35,36]. The use of these data for modeling allows for a detailed analysis of the obtained measurement results [25,26]. An essential problem in the production process is to identify and select the important factors affecting its stability [34]. This allows an evaluation of the current condition and implementation of the solutions to compensate the disturbance, if it is identified [4,17,23]. A separate issue is to conduct laboratory test to determine the strength of individual components. Based on this and with the use of statistical tools,

(*) Corresponding author.
E-mail addresses:

W. Zębala (ORCID: 0000-0002-5590-1338) wojciech.zebala@pk.edu.pl, S. Młynarski (ORCID: 0000-0002-3374-7739) stanislaw.mlynarski@pk.edu.pl, Ł. Ślusarczyk (ORCID: 0000-0002-3565-7868) lukasz.slusarczyk@pk.edu.pl,

an approach rationalizing the operation of technical systems is determined [16,30,31].

Much work is being carried out to obtain appropriate indicators of the durability of abrasive tools. The article [1] presents the results of experimental research on the phenomenon of chip accumulation on the active surface of a ceramic grinding wheel with CBN grains during grinding of nickel alloys. Reducing the cutting capacity of the grinding wheel leads to the high cutting forces and an increase in temperature in the cutting zone. The authors presented an analytical model describing the influence of the cutting parameters and grinding wheel design on the adhesion of chips to the active surface of the grinding wheel. Nadolny [21] analyzed the wear process of the active surface of a grinding wheel with different volumes of a ceramic binder with a glass-crystalline structure and sintered corundum grains. During experimental tests, bearing rings made of 100Cr6 steel (62 HRC) were ground. The results of the tests showed that the increase in the volume of bonds translated into lower abrasive wear of CPS.

Another direction of research is to maintain the integrity of the grinding wheel during roughing and finishing. The article [8] examined the influence of the glass transition of the grinding wheel on the development of strength between abrasive grains and connecting bridges, as well as the nature of the cracking and wear of vitrified grinding wheels used for precision grinding. The article [27] presents an approach to reducing operating costs by using conventional grinding wheels with ceramic grains and a binder with high retention and a lower bond to abrasive ratio. The adopted solution was assessed using the Dooly method, where its effectiveness was demonstrated. A separate, important group of studies on the grinding wheel operation process is the analysis of the physical phenomena in the cutting zone. Rasim et al. [24] used a high-speed camera to analyze the work of a single CBN abrasive grain during grinding of AISI 5210 hardened steel. Based on the results obtained, the phases of the chip formation and abrasive grain cavities were defined. The authors proposed a quantitative model of the chip formation that takes into account the three-dimensional shape of the grains as well as the cutting speed and cooling conditions in the cutting zone. A similar topic was discussed

by Kacalak et al. [9]. The interaction between a single abrasive grain and the workpiece has been divided into three stages, where the share of each stage depends on the properties of the workpiece, grinding parameters, the state of friction between the abrasive grain and the workpiece and the shape of the grains. The article presents the results of the numerical and experimental grinding process of the Ti-6Al-4V titanium alloy using a conventional grinding wheel and a newly developed grinding wheel with grain aggregates. The influence of the geometric parameters of abrasive grains and aggregates in the direction of movement and in the transverse direction on the size of the ridges was determined.

An innovative approach to the construction of a grinding wheel was described in work [15]. The finishing grinding process of the Inconel 625 alloy was performed using a grinding wheel with an innovative design consisting of grains of various sizes, which resulted in less damage to the working surface and improved production process. The authors [2] used ANN to analyze the wear state of the grinding wheel and determine the surface quality of the workpiece. An important element of the proposed concept is the use of a virtual sensor which, after validation, is able to analyze the relationship between measured parameters and the power consumption on the grinder spindle.

The purpose of the grinding process is to remove the machining allowance of the workpiece by micro-cutting [8,9,27]. Modeling and simulation of phenomena occurring in the cutting zone using numerical methods has been described in [7,32]. In [7] the results of kinematic simulations of the operation of a grinding wheel with CBN grains for various parameters of the grinding process are presented. The wear condition of the grinding wheel was taken into account by reducing the grain exposure height. The results of the conducted simulation tests correspond well with the experiment. Paper [32] focused on precision grinding of parts based on brittle materials. Simulation and experimental research concerned the machining of optical lenses with a CBN grinding wheel. The influence of multiple passes of the grinding wheel through the same area of the machined surface on the change in the surface topography was determined. Both studies confirm that there is high stochasticity in the studied grinding process, and the complexity of the workpiece surface

gradually increases with the number of passes. The intensively operating tribological pair as a tribological system is located in areas where the highest friction coefficient for technically dry friction should occur. Dry friction occurs when there are no foreign bodies, such as grease or water, between the mating surfaces. This type of friction is a complex phenomenon and depends on many factors [13,22,33]. This is accompanied by the formation of stresses, wear of friction materials and heat generation.

Abrasive wear as a dynamic process involves changing the surfaces of bodies in motion relative to each other as a result of the mechanical interaction between them. This process depends on many factors and parameters, such as the geometry of the contacting surfaces, the applied normal force, the sliding speed and the hardness of the material [19,22]. Many studies concern the important issue of temperature measurement in the cutting zone during the grinding process. Paper [19] presents an overview of analytical methods for calculating grinding temperatures and their impact on thermal damage. The authors raise the important problem of heat partition between the workpiece and the abrasive grains. Analytical models have been proposed that describe the energy distribution in the grinding zone for various grinding wheel operating parameters, taking into account the thermal conductivity of abrasive grains. The article [13] addresses the issue of the influence of workpiece speed, cutting depth and grinding wheel speed on the workpiece temperature during conventional dry surface grinding. Temperature measurement at various depths of the ground surface was carried out with high accuracy thanks to the use of a thin layer of PVD foil deposited on the workpiece as a thermal sensor. The conducted research made it possible to determine the maximum temperature increase and to correlate the temperature gradient with the residual stresses induced on the surface. The properties of a lamellar abrasive disc can be modeled based on wear processes resulting from operating conditions, the environment and other external factors. It is important to determine the parameter characterizing the operation of the abrasive tool, which is most sensitive to changes related to damage. This parameter should be representative of all tested performance properties [33]. Operational practice indicates the assessment of the technical

condition based on the analysis of numerical values of the control parameters that characterize the wear processes of the tool and its components and have a degressive effect on the tool design [3].

In this paper, the specialized program Weibull++ was used to estimate the results of the empirical research. The developed models of probability distributions of the examined indicators values obtained from the estimation of the empirical data provided a range of information about the causes of the processes taking place as well as the properties and features of the tested tools. Selected results are presented in the further part of the study in the form of graphical characteristics and analytical models of functional relationships between the tested parameters and the properties of the manufactured tools. The second part of the paper presents the results of research verifying the developed scientific model in the context of the exploitation process of lamellar grinding wheels. On a specially prepared test stand, non-contact temperature measurement was carried out in the grinding zone with new and worn grinding wheels, for different values of the load of the grinding wheel on the workpiece and different values of the working angle of the grinding wheel.

2. MATHEMATICAL MODELS DESCRIBING THE WEAR OF THE BACKGROUND DISCS

The components of the background disc construction include dispersed reinforcements (e.g. pieces of fiberglass or polyethylene chips), external reinforcements in the form of a mesh on the upper and lower surfaces of the composite, and fillers such as quartz sand, calfix and barite. Accurate measurement of the amount of individual components allows to obtain backgrounds with different properties and to experiment with compositions and mixing parameters in order to obtain optimal properties of the finished product. Each change of quartz sand granulation or resin type requires correction of both the content of individual components and the parameters of the mixing process.

The subsequent phases of the research process enabled the development of procedures for improving the production technology, including the composition of materials, which were differentiated in terms of the basis weight of the

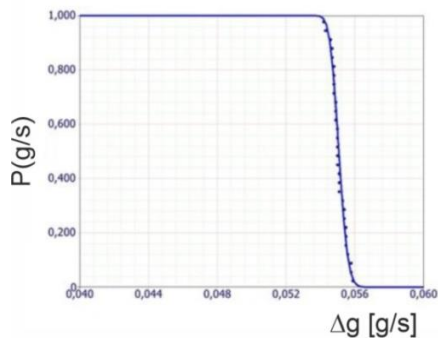
fractions of materials and fillers used to obtain a more homogeneous structure. The test results obtained for the samples admitted for further testing were used to determine the probability and the probability density of the value of the disc mass and thickness measure. These data enable a probabilistic approach to assessing production repeatability [14].

The introduction of successive changes in the design of discs and the verification of the mathematical probabilistic models determining the impact of these changes on design and operational indicators made it possible to obtain knowledge to develop a technological process in which all discs from the tested sample meet the requirements of post-production conformity assessment (finish, structure quality, dimensional accuracy, balancing) and operational security. Subsequent series of produced discs were tested for bursting in the entire range of rotational speeds of the testing device up to 180 m/s. The results of the tests gave rise to the development of the disc design and technology for its production, for which all of the tested sample of manufactured discs obtained positive results in bursting tests.

2.1. Material

Four backgrounds with different material composition were

1. Code of background PL29 115X2,5 3 1 2



selected for the experimental determination of the wear of the background disks. The backgrounds marking method is presented below:

Table 1. Codes of backgrounds selected for further tests.

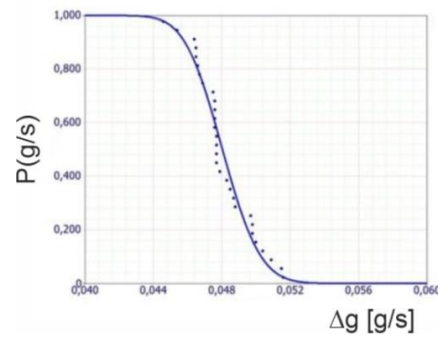
| Backgrounds for lamellas | Shape | Dimensions | No of sample | No of mixture | Graph number* |
|--------------------------|-------|------------|--------------|---------------|---------------|
| PL | 29 | 115X4,0 | 4A | 1 | 2 |
| PL | 29 | 115X4,0 | 4B | 1 | 2 |
| PL | 29 | 115X4,0 | 4B | 2 | 2 |
| PL | 29 | 115X4,0 | 3 | 1 | 2 |

*(temperature curve for background hardening)

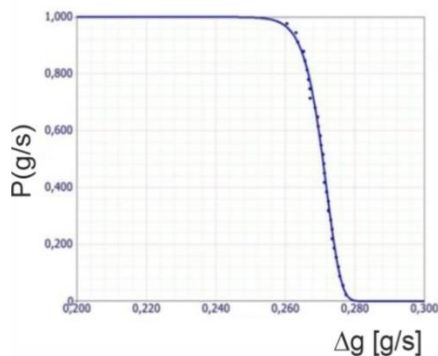
2.2. Research of background wear

The results of the wear tests were estimated and the models and parameters of the wear probability distribution expressed in [g/s] were determined. In all tests, a constant pressing force of the background pad was assumed. Wear probability distributions were modeled with two models: Gamma and Generalized Gamma. Fig. 1 shows the wear characteristics of the background discs expressed in [g/s] for various compositions of the resin and filler of the background material. The collective list of characteristics graphically presents the differentiation of the wear properties of the disc background.

2. Code of background PL29 115X4,0 4B 1 2



3. Code of background PL29 115X4,0 4B 2 2



4. Code of background PL29 115X4,0 4A 1 2

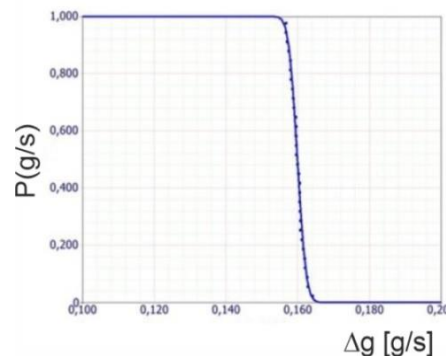


Fig. 1. Wear characteristics of background discs expressed in [g/s] for different construction material compositions.

On the basis of the obtained results, the values of the operational wear intensity index were determined with the probability $P(R=0.95)$, Table 2.

Table 2. Wear intensity indicator.

| | Code of background | Intensity of operational wear |
|---|---------------------|----------------------------------|
| 1 | PL29 115X2,5 3 1 2 | $P(R=0,95) = 0,0544 \text{ g/s}$ |
| 2 | PL29 115X4,0 4B 1 2 | $P(R=0,95) = 0,0452 \text{ g/s}$ |
| 3 | PL29 115X4,0 4B 2 2 | $P(R=0,95) = 0,2616 \text{ g/s}$ |
| 4 | PL29 115X4,0 4A 1 2 | $P(R=0,95) = 0,1568 \text{ g/s}$ |

This information is an important element in the research process and will be used to further conclusions about the operational properties of the finished flap discs, including the construction of a mathematical model for verifying the properties of the base materials used for the production of the flap disc background. The next stage of the experimental research concerned the determination of the wear, depending on the percentage content of the filler (Table 3, Fig. 2).

Table 3. Test results of the background wear depending on the filler content.

| | Code of background | Wear Z [g/s] | Filler W [%] |
|---|---------------------|--------------|--------------|
| 1 | PL29 115X4,0 4B 1 2 | 0,0452 | 40 |
| 2 | PL29 115X2,5 3 1 2 | 0,0544 | 50 |
| 3 | PL29 115X4,0 4A 1 2 | 0,1567 | 60 |
| 4 | PL29 115X4,0 4B 2 2 | 0,2615 | 70 |

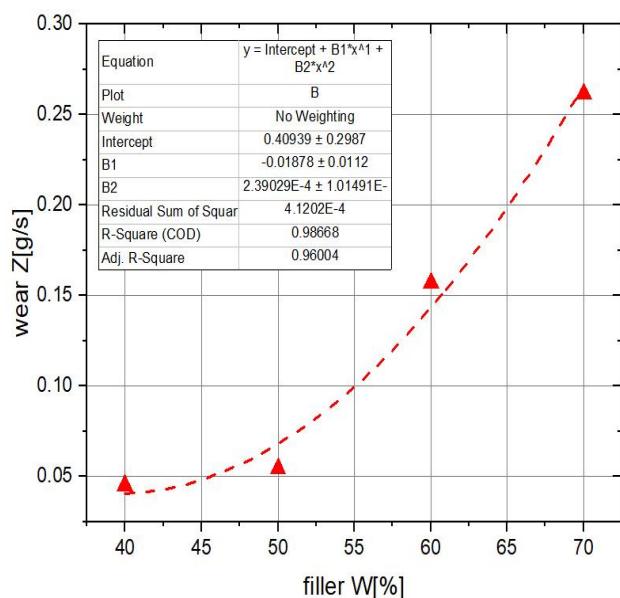


Fig. 2. Wear characteristics of the complete grinding wheel as a function of the filler content.

Based on the obtained results, it can be concluded that a higher filler content results in the faster wear of the disc background. Experimental studies related to the wear of the

abrasive wheel background during operation provided the results of wear Z expressed in [g/s]. The results obtained for various compositions of the filler material in the disc construction show that the wear depends on the composition of the construction material. This dependence makes it possible to determine the correct composition of the material to obtain the planned wear of the grinding wheel.

The mathematical model of the background wear was described by a 2nd degree polynomial (2):

$$Z(W) = 2,39 \cdot W^2 - 0,1878 \cdot W + 0,4094 \quad (2)$$

2.3. Burst resistance test of backgrounds

Examination of abrasive discs during operation provided information to determine the limit operating speeds of the disc depending on the composition of the construction material (Table 3, Fig. 3).

Table 3. Test results of the burst resistance of the grinding wheel backgrounds.

| | Code of disc | v [m/s] | Resin S [%] |
|----|---------------------|---------------------|-------------|
| 1 | PL29 115X4,0 4B 1 2 | $V(R=0,95) = 128,9$ | 9 |
| 2 | PL29 115X2,5 3 1 2 | $V(R=0,95) = 129,9$ | 10 |
| 3 | PL29 115X4,0 4A 1 2 | $V(R=0,95) = 138,7$ | 12 |
| 4 | PL29 115X2,5 3 1 2 | $V(R=0,95) = 139,2$ | 14 |
| 5 | PL29 115X4,0 4A 1 2 | $V(R=0,95) = 145,0$ | 16 |
| 6 | PL29 115X2,5 3 1 2 | $V(R=0,95) = 140,3$ | 18 |
| 7 | PL29 115X4,0 4B 1 2 | $V(R=0,95) = 161,4$ | 19 |
| 8 | PL29 115X2,5 3 1 2 | $V(R=0,95) = 151,7$ | 20 |
| 9 | PL29 115X4,0 4B 2 2 | $V(R=0,95) = 172,1$ | 21 |
| 10 | PL29 115X4,0 4B 2 2 | $V(R=0,95) = 186,7$ | 22 |

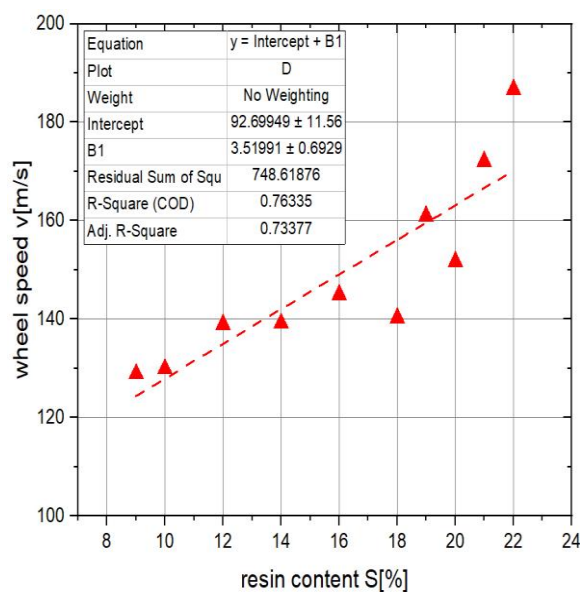


Fig. 3. Characteristics of the burst resistance of the grinding wheel background as a function of the resin content and wheel speed.

The presented dependence makes it possible to determine the composition of the material to obtain the safe standard working speeds v [m/s].

The mathematical model of the burst resistance of the disc background is described by linear polynomial (3):

$$v(S) = 3,52 \cdot S + 92,7 \quad (3)$$

2.4. Testing the quality of glue connections of leaves with the grinding wheel

The next stage of testing abrasive wheels during operation is the functional dependence to determine the limit speed of the wheel operation depending on the size of the glue dose used to connect the lamella with the construction material of the wheel (Table 4, Fig. 4).

Table 4. The results of the disc speed limit tests depending on the adhesive dose.

| | Code of disc | Glue weight [g] | v [m/s] |
|---|---------------------|-----------------|-----------|
| 1 | PL29 115X4,0 4A 1 2 | 9 | 94,9 |
| 2 | PL29 115X4,0 4A 1 2 | 12 | 118,5 |
| 3 | PL29 115X4,0 4A 1 2 | 14 | 175,8 |
| 4 | PL29 115X4,0 4A 1 2 | 16 | 184,2 |
| 5 | PL29 115X4,0 4B 2 2 | 18 | 189,4 |

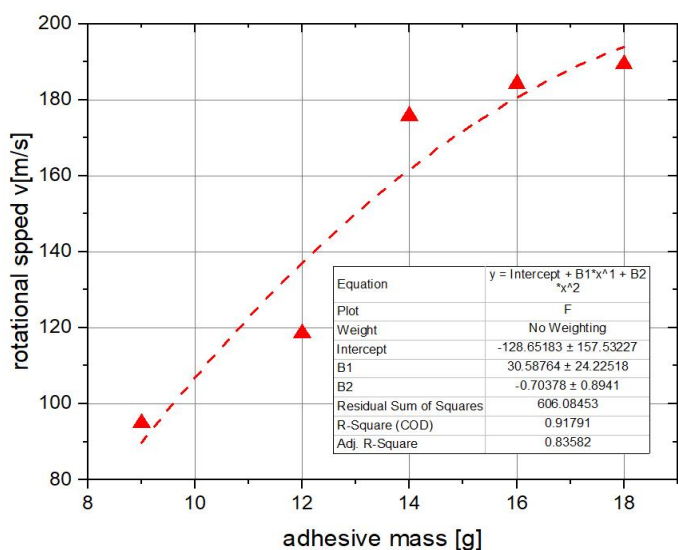


Fig. 4. Characteristics of the burst resistance of the adhesive connection of the leaves with the grinding wheel as a function of the adhesive mass (glue weight) and the rotational speed of the disc.

The mathematical model of burst resistance was described by a 2nd degree polynomial (4):

$$v(k) = -0,7038 \cdot k^2 + 30,588 \cdot k - 128,65 \quad (4)$$

2.5. Burst resistance test depending on the leaves abrasive granules

The next stage of the research was to determine the limit speed of the disc due to the granulation of the lamellae abrasive. This dependence makes it possible to determine the safe limit speed of the tool operation expressed in [m/s] of the manufactured flap discs. A random group of backgrounds was used to test the burst resistance of the complete lamellar grinding wheel (Table 5, Fig. 5).

Table 5. The results of the burst resistance tests of the complete grinding wheel depending on the granulation of the abrasive leaves.

| | Code of disc | Granulation | v [m/s] |
|----|---------------------|-------------|-----------|
| 1 | PL29 115X4,0 4A 1 2 | 40 | 118,5 |
| 2 | PL29 115X2,5 3 1 2 | 40 | 116,3 |
| 3 | PL29 115X4,0 4A 1 2 | 40 | 89,60 |
| | Code of disc | Granulation | v [m/s] |
| 4 | PL29 115X4,0 4A 1 2 | 40 | 117,2 |
| 5 | PL29 115X4,0 4A 1 2 | 50 | 118,0 |
| 6 | PL29 115X4,0 4B 1 2 | 50 | 110,9 |
| 7 | PL29 115X4,0 4A 1 2 | 50 | 149,5 |
| 8 | PL29 115X2,5 3 1 2 | 50 | 111,6 |
| 9 | PL29 115X4,0 4A 1 2 | 60 | 148,4 |
| 10 | PL29 115X2,5 3 1 2 | 60 | 148,4 |
| 11 | PL29 115X4,0 4B 1 2 | 60 | 148,3 |
| 12 | PL29 115X4,0 4A 1 2 | 60 | 148,7 |
| 13 | PL29 115X4,0 4B1 2 | 60 | 179,0 |

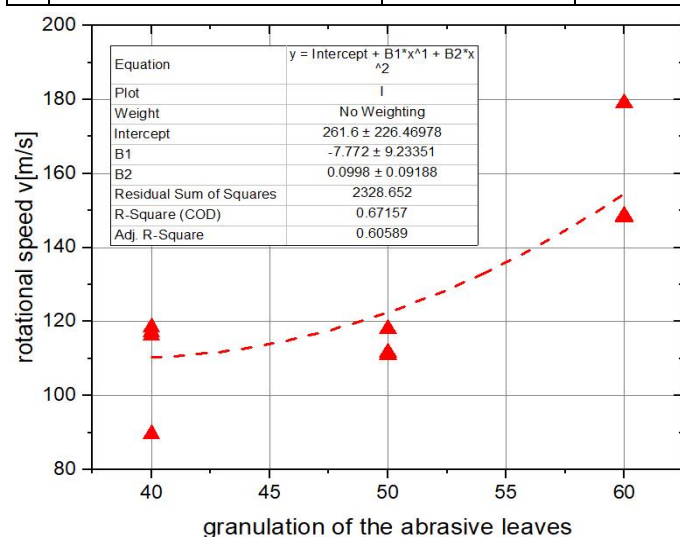


Fig. 5. Characteristics of the tool's resistance to destruction as a function of the speed and granulation of the abrasive leaves.

The mathematical model of the tool's resistance to damage as a function of speed and granulation of the abrasive leaves is described by a 2nd degree polynomial (5):

$$v(g) = 0,0998 \cdot g^2 - 7,772 \cdot g + 261,6 \quad (5)$$

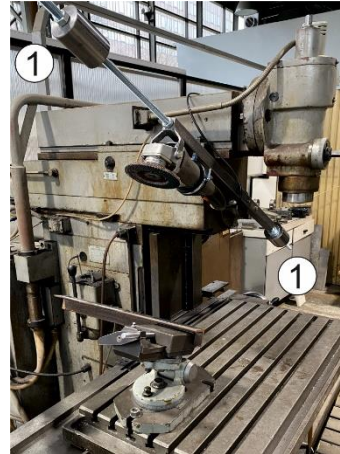
Four backgrounds were selected for further tests: PL29 115X2.5 3 1 2; PL29 115X4.0 4B 1 2; PL29 115X4.0 4B 2 2 and PL29 115X4.0 4A 1 2. The selected backgrounds ensured a safe operation within the range of tested parameters.

3. DETERMINATION OF THE TEMPERATURE IN THE GRINDING ZONE

A manual 3-axis milling machine was adapted for the



a)



b)

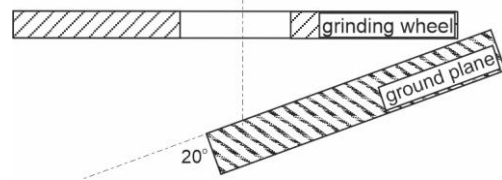
Fig. 6. View of the station - angle grinder assembly method (1 - weights marking).

The design of the test stand also made it possible to change the load value of the grinding wheel on the ground surface. Fig. 6b shows the applied solution. Weights with the possibility of changing the position mounted on the ends of the arm (marked in the figure with the number 1) allowed to

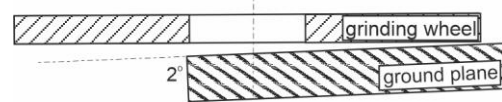
construction of the test stand. An angle grinder with a power of 900 W and a maximum speed of 11,000 rpm was used for the grinding tests. Fig. 6 shows the method of mounting the grinder on the test stand. Thanks to this solution, it was possible to grind the surface with a constant feed, using the mechanical feed of the milling table in the Y axis (Fig. 6a). The workpiece during the tests was a hot-rolled angle bar 40x40x5 made of ST3S steel.



adjust the load of the grinding wheel on the workpiece. The angle change between the working plane of the grinding wheel and the ground plane was carried out by changing the angular setting of the vice. Fig. 7 shows two vise settings: in Fig. 7a, the angle was 20°, and in Fig. 7b, the angle was 2°.



a)



b)

Fig. 7. Setting the angle between the working plane of the grinding wheel and the ground plane: a) the angle is 20°, b) the angle is 2°.

The infrared camera used during the research worked with an optical resolution of 640x480 px. Table 6 shows the configuration parameters of the camera during the basic tests

Table 6. Configuration parameters of the infrared camera during tests

| | |
|---------------------------|----------------------|
| Model of camera | FLIR SC 620 |
| Thermal lens | Fixed focus, f=38 mm |
| Object distance | 1.0 m |
| The emissivity of surface | $\epsilon=0.6$ |

| | |
|---------------------|------------|
| Ambient temperature | 20 °C |
| Optical resolution | 640x480 px |
| Registration rate | 30 f/s. |

The infrared camera was connected to a PC. The registration and analysis of the thermal imaging sequences was carried out in the specialized computer programs ThermoCamResearcher PRO 2.9 and FLIR Tools. The recording time of the thermovision sequence was about 8 seconds and allowed to determine the average contact temperature in the processing zone. Four types of lamellar grinding wheels (marked A-40; Z-40; Z-60; P-60) built on different backgrounds discs with a diameter of 115 mm were used to determine the temperature in the grinding zone. (Table 7).

Table 7. Characteristics of the backgrounds used in the tests.

| No | Disc code | Grinding wheel |
|----|---------------------|----------------|
| 1 | PL29 115X4,0 4B 1 2 | A-40 115 |
| 2 | PL29 115X2,5 3 1 2 | Z-40 115 |
| 3 | PL29 115X4,0 4A 1 2 | Z-60 115 |
| 4 | PL29 115X4,0 4B 2 2 | P-60 115 |

On the basis of the preliminary research, it was established that grinding tests should be carried out with a feed rate of $f=500$ mm/min relative to the machined surface. In addition, the experimentally determined setting of the infrared camera enabled the observation of the machining zone and the determination of the contact temperature between the working plane of the lamellar grinding wheel and the ground surface. The basic research plan was developed according to the Taguchi method. The independent variables were the angle of the grinding wheel (the angle between the working plane of the grinding wheel and the ground plane), the load of the

grinding wheel on the ground surface and the degree of grinding wheel wear. Parameter values are presented in Table 8.

Table 8. The range of variability of grinding wheel operating parameters during basic tests.

| Symbol | Parameter | Variable designation | Parameter value | |
|--------|----------------------------------|----------------------|-----------------|-----------------|
| A | Grinding wheel working angle [°] | Ks | 2 | 20 |
| B | Grinding wheel load [kg] | Ns | 1 | 3 |
| C | Degree of wear [-] | Sz | new symbol (1) | worn symbol (2) |

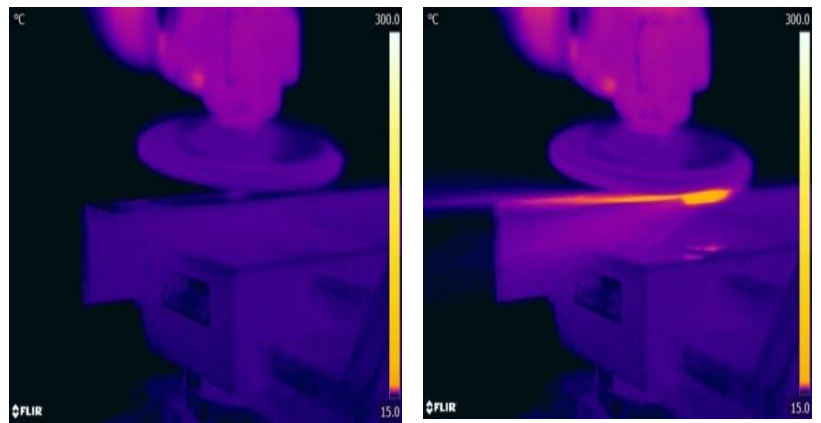
The value of the parameter Sz, defining the degree of wear of the grinding wheel as worn (2), was assumed for the visibly worn abrasive material on the lamellae, which corresponded to the grinding wheel operation time of 20 minutes. For each of the four tested grinding wheels, 8 grinding tests were performed. A total of 32 trials were performed. Table 9 presents the processing parameters adopted for each test.

Table 9. Values of grinding wheel operating parameters for each test.

| Test number | A | B | C | The angle of the grinding wheel [°] | Grinding wheel load [kg] | Degree of wear [-] |
|-------------|---|---|---|-------------------------------------|--------------------------|--------------------|
| 1 | 1 | 1 | 1 | 2 | 1 | 1 |
| 2 | 1 | 1 | 2 | 2 | 1 | 2 |
| 3 | 1 | 2 | 1 | 2 | 3 | 1 |
| 4 | 1 | 2 | 2 | 2 | 3 | 2 |
| 5 | 2 | 1 | 1 | 20 | 1 | 1 |
| 6 | 2 | 1 | 2 | 20 | 1 | 2 |
| 7 | 2 | 2 | 1 | 20 | 3 | 1 |
| 8 | 2 | 2 | 2 | 20 | 3 | 2 |

4. ANALYSIS OF THE RESULTS

An example of time-lapse analysis of the thermal imaging sequence during the operation of the Z-60 grinding wheel is shown below in Fig. 8.



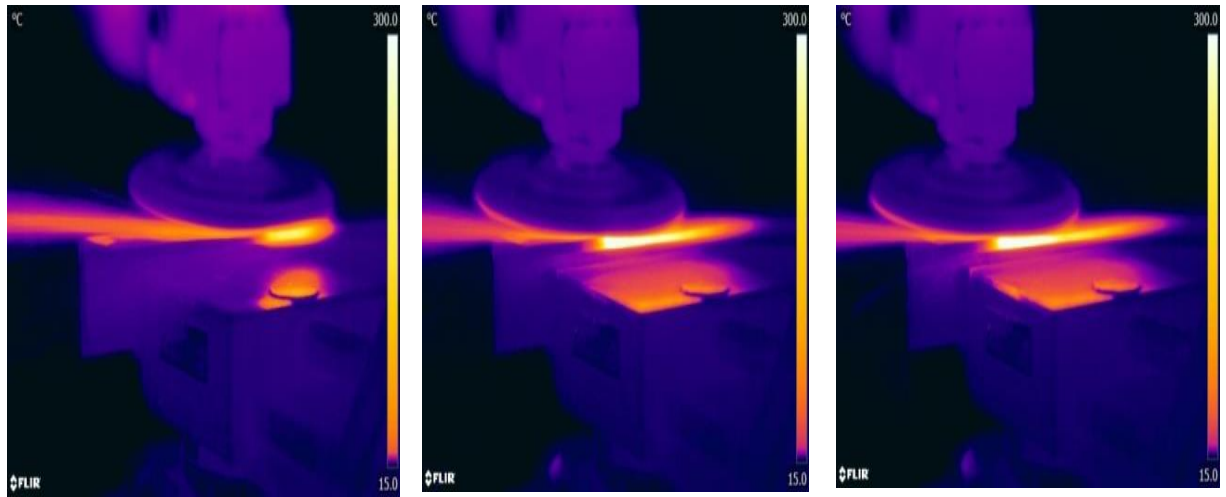


Fig. 8. Time-lapse analysis of the thermal imaging sequence while working with the Z-60 grinding wheel.

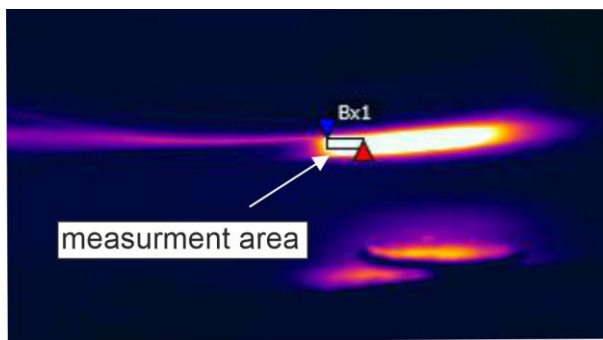


Fig. 9. Contact temperature measurement area during basic tests.

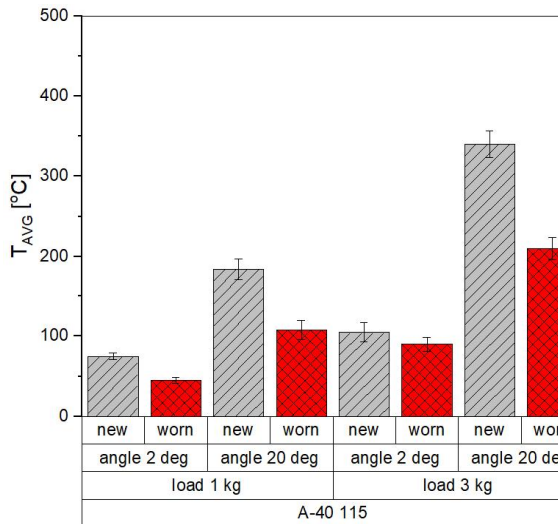
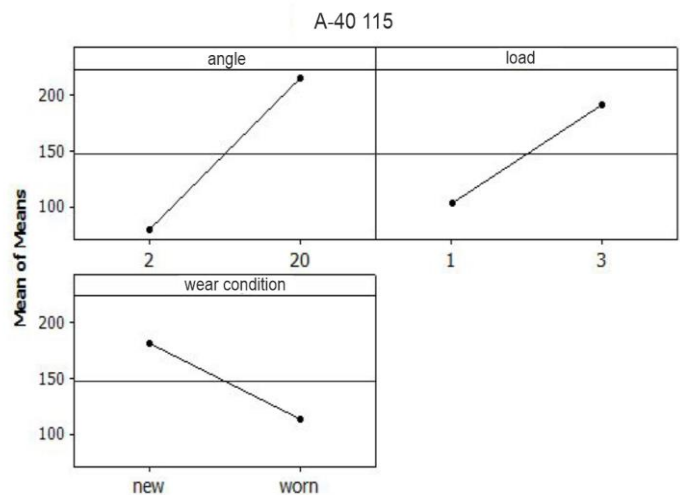


Fig. 10. The dependence of temperature T_{AVG} on the operating parameters of the grinding wheel A-40.

The determined Mean of Means relationships present the impact of the three independent variables: grinding wheel inclination angle, grinding wheel pressure, and the wear condition on the mean temperature. Increase of the grinding wheel inclination angle and the grinding wheel pressure increases the temperature in the grinding zone. The grinding wheel wear decreases the temperature in the grinding zone.

The contact temperature was measured inside the control object in the shape of a rectangle, 3x8 mm in size, Fig. 9. The analysis of the recorded thermal imaging sequences enabled the determination of the average contact temperature, T_{AVG} .

Fig. 10 shows the dependence of the average temperature T_{AVG} on the operating parameters of the A-40 grinding wheel.



At the stage of the statistical analysis of the results, the S/N ratio was determined. The criterion was adopted - the lower the better. According to Taguchi model, this type of factor is used when it is desirable to minimize some of the undesirable characteristics of the product. The S/N ratio was calculated from the formula (6):

$$\frac{S}{N} = -10 \cdot \log \left(\frac{1}{n} \sum_{i=1}^n y_i^2 \right) \quad (6)$$

where: y- measured feature, n- number of measurements

The results of statistical analysis obtained for the A-40 grinding wheel are presented in Table 10 and Table 11.

Table 10. Statistical analysis results obtained for the grinding wheel A-40.

| Test number | K_s [°] | N_s [kg] | S_z [-] | S/N | T_{AVG} [°] |
|-------------|-----------|------------|-----------|--------|---------------|
| 1 | 2 | 1 | new | -37,50 | 75 |
| 2 | 2 | 1 | worn | -33,07 | 45 |
| 3 | 2 | 3 | new | -40,42 | 105 |
| 4 | 2 | 3 | worn | -39,08 | 90 |
| 5 | 20 | 1 | new | -45,29 | 184 |
| 6 | 20 | 1 | worn | -40,66 | 108 |
| 7 | 20 | 3 | new | -51,12 | 340 |
| 8 | 20 | 3 | worn | -46,44 | 210 |

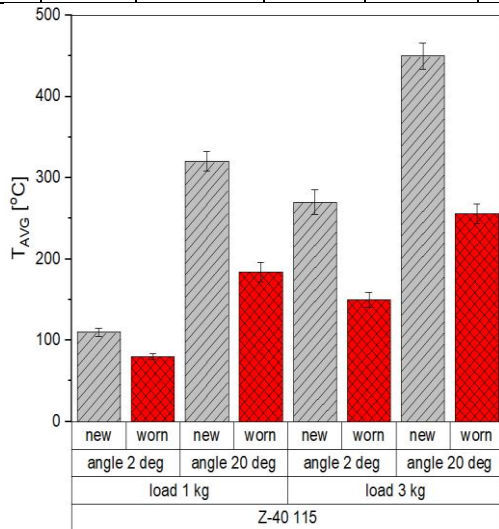


Fig. 11. The dependence of temperature T_{AVG} on the operating parameters of the grinding wheel Z-40.

The results of statistical analysis obtained for the Z-40 grinding wheel are presented in the Tables 12 and 13.

Table 12. Statistical analysis results obtained for the grinding wheel Z-40.

| Test number | K_s [°] | N_s [kg] | S_z [-] | S/N | T_{AVG} [°] |
|-------------|-----------|------------|-----------|--------|---------------|
| 1 | 2 | 1 | new | -40,82 | 110 |
| 2 | 2 | 1 | worn | -38,06 | 80 |
| 3 | 2 | 3 | new | -48,62 | 270 |
| 4 | 2 | 3 | worn | -43,52 | 150 |
| 5 | 20 | 1 | new | -50,10 | 320 |
| 6 | 20 | 1 | worn | -45,29 | 184 |
| 7 | 20 | 3 | new | -53,06 | 450 |
| 8 | 20 | 3 | worn | -48,16 | 256 |

The regression equation of the average contact

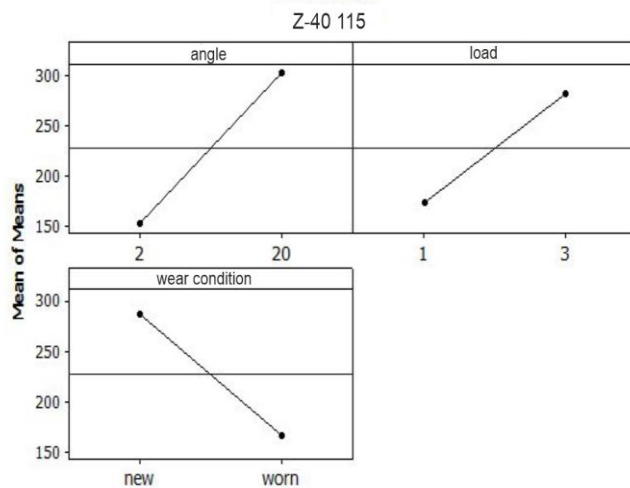
temperature T_{AVG} for the grinding wheel A-40 (7):

$$T_{AVG}(K_s, N_s, S_z) = 76,9306 + 7,5972 \cdot K_s + 44,125 \cdot N_s - 67,75 \cdot S_z \quad (7)$$

Table 11. The analysis of variance of temperature T_{AVG} for the grinding wheel A-40.

| Source | DF | Seq SS | Adj SS | Adj MS | F | p |
|----------------|----|---------|---------|---------|-------|-------|
| K_s | 1 | 55240,4 | 55240,4 | 55240,4 | 85,28 | 0,000 |
| N_s | 1 | 788 | 736,8 | 736,8 | 1,14 | 0,297 |
| S_z | 1 | 2557,6 | 2557,6 | 2557,6 | 3,95 | 0,059 |
| Residual error | 23 | 14899 | 14899 | 647,8 | | |
| Total | 26 | 73485,1 | | | | |

Fig. 11 shows the dependence of the average T_{AVG} temperature on the operating parameters of the grinding wheel Z-40.



temperature T_{AVG} for the grinding wheel Z-40 (8):

$$T_{AVG}(K_s, N_s, S_z) = 207,833 + 8,333 \cdot K_s + 54,000 \cdot N_s - 120,000 \cdot S_z \quad (8)$$

Table 13. The analysis of variance of temperature T_{AVG} for the grinding wheel Z-40.

| Source | DF | Seq SS | Adj SS | Adj MS | F | p |
|----------------|----|---------|---------|---------|-------|-------|
| K_s | 1 | 55240,4 | 55240,4 | 55240,4 | 85,28 | 0,000 |
| N_s | 1 | 788 | 736,8 | 736,8 | 1,14 | 0,297 |
| S_z | 1 | 2557,6 | 2557,6 | 2557,6 | 3,95 | 0,059 |
| Residual error | 23 | 14899 | 14899 | 647,8 | | |
| Total | 26 | 73485,1 | | | | |

Fig. 12 shows the dependence of the average T_{AVG} temperature on the operating parameters of the grinding wheel Z-60.

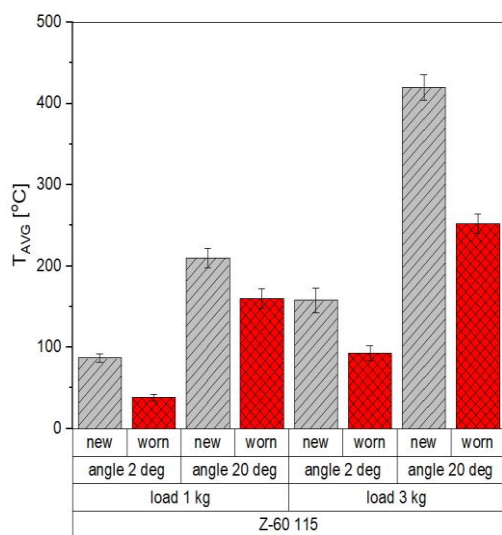


Fig. 12. The dependence of temperature T_{AVG} on the operating parameters of the grinding wheel Z-60.

The results of statistical analysis obtained for the Z-60 grinding wheel are presented in the Tables 14 and 15.

Table 14. Statistical analysis results obtained for the grinding wheel Z-60.

| Test number | K_s [°] | N_s [kg] | S_z [-] | S/N | T_{AVG} [°] |
|-------------|-----------|------------|-----------|--------|---------------|
| 1 | 2 | 1 | new | -38,79 | 87 |
| 2 | 2 | 1 | worn | -31,59 | 38 |
| 3 | 2 | 3 | new | -43,97 | 150 |
| 4 | 2 | 3 | worn | -39,36 | 93 |
| 5 | 20 | 1 | new | -46,44 | 210 |
| 6 | 20 | 1 | worn | -44,08 | 160 |
| 7 | 20 | 3 | new | -52,86 | 430 |
| 8 | 20 | 3 | worn | -48,02 | 252 |

The regression equation of the average contact

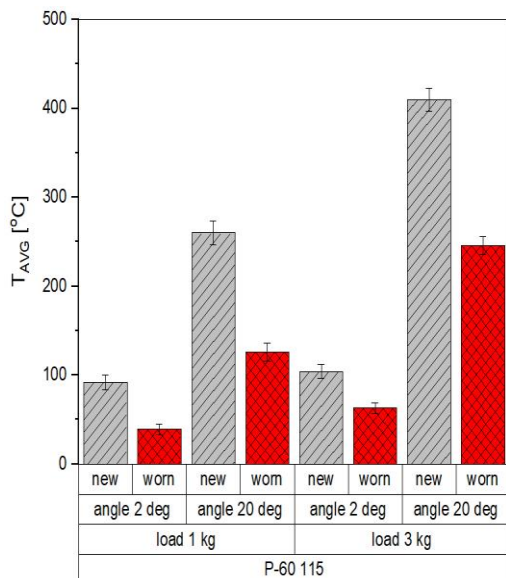
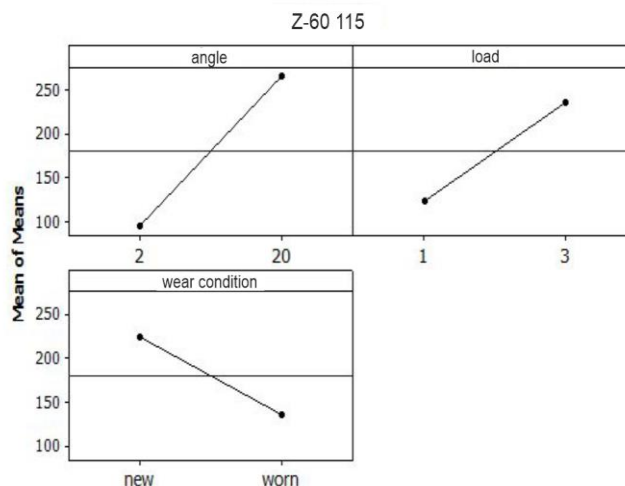


Fig. 13. The dependence of temperature T_{AVG} on the operating parameters of the grinding wheel P-60.

The results of statistical analysis obtained for the P-60 grinding wheel are presented in Tables 16 and 17.



temperature T_{AVG} for the grinding wheel Z-60 (9):

$$T_{AVG}(K_s, N_s, S_z) = 94,9444 + 9,5277 \cdot K_s + 56,00 \cdot N_s - 88,00 \cdot S_z \quad (9)$$

Table 15. The analysis of variance of temperature T_{AVG} for the grinding wheel Z-60.

| Source | DF | Seq SS | Adj SS | Adj MS | F | p |
|----------------|----|---------|---------|---------|-------|-------|
| K_s | 1 | 55240,4 | 55240,4 | 55240,4 | 85,28 | 0,000 |
| N_s | 1 | 788 | 736,8 | 736,8 | 1,14 | 0,297 |
| S_z | 1 | 2557,6 | 2557,6 | 2557,6 | 3,95 | 0,059 |
| Residual error | 23 | 14899 | 14899 | 647,8 | | |
| Total | 26 | 73485,1 | | | | |

Fig. 13 shows the dependence of the average T_{AVG} temperature on the operating parameters of the grinding wheel P-60.

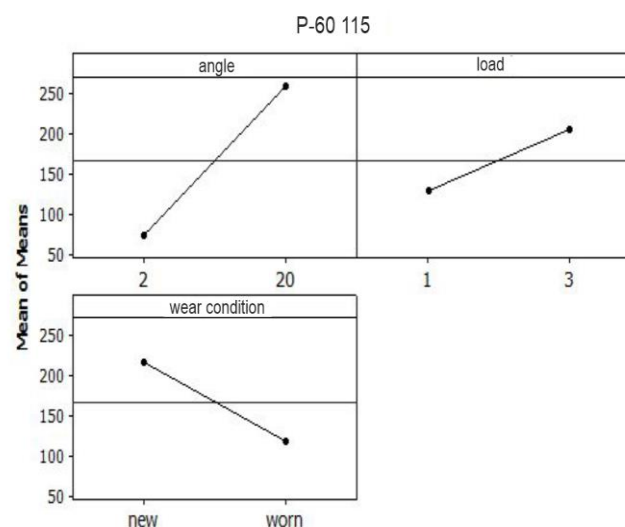


Table 16. Statistical analysis results obtained for the grinding wheel P-60.

| Test number | K_s [°] | N_s [kg] | S_z [-] | S/N | T_{AVG} [°] |
|-------------|-----------|------------|-----------|--------|---------------|
| 1 | 2 | 1 | new | -39,27 | 92 |
| 2 | 2 | 1 | worn | -31,82 | 39 |
| 3 | 2 | 3 | new | -40,34 | 104 |
| 4 | 2 | 3 | worn | -35,98 | 63 |
| 5 | 20 | 1 | new | -48,29 | 260 |
| 6 | 20 | 1 | worn | -42,00 | 126 |
| 7 | 20 | 3 | new | -52,25 | 410 |
| 8 | 20 | 3 | worn | -47,81 | 246 |

The regression equation of the average contact temperature T_{AVG} for the grinding wheel P-60 (10):

$$T_{AVG}(K_s, N_s, S_z) = 124,333 + 10,333 \cdot K_s + 38,00 \cdot N_s - 98,00 \cdot S_z \quad (10)$$

Table 17. The analysis of variance of temperature T_{AVG} for the grinding wheel P-60.

| Source | DF | Seq SS | Adj SS | Adj MS | F | p |
|--------|----|---------|---------|---------|-------|-------|
| K_s | 1 | 55240,4 | 55240,4 | 55240,4 | 85,28 | 0,000 |
| N_s | 1 | 788 | 736,8 | 736,8 | 1,14 | 0,297 |
| S_z | 1 | 2557,6 | 2557,6 | 2557,6 | 3,95 | 0,059 |
| Source | DF | Seq SS | Adj SS | Adj MS | F | p |



| Source | DF | Seq SS | Adj SS | Adj MS | F | p |
|----------------|----|---------|--------|--------|---|---|
| Residual error | 23 | 14899 | 14899 | 647,8 | | |
| Total | 26 | 73485,1 | | | | |

Due to the design of the tested lamellar grinding wheels, characteristic courses of the dependence T_{AVG} on the grinding wheel operation time were observed, example in Fig. 14. In the first phase of the grinding with the new grinding wheel, the outer part of the lamellas works, which corresponds to the highest value of the cutting speed. After the outer part is worn, the second grinding phase takes place, in which the inner part of the lamella works. The second phase of the grinding wheel operation is associated with a decrease of the cutting speed. In the first phase of the grinding wheel operation, an increase of T_{AVG} was observed with the achievement of the maximum value of T_{MAX} in the grinding process, while in the second phase

a slight decrease and stabilization of T_{AVG} were observed. The observed relationship results from the innovative design of the grinding wheel.

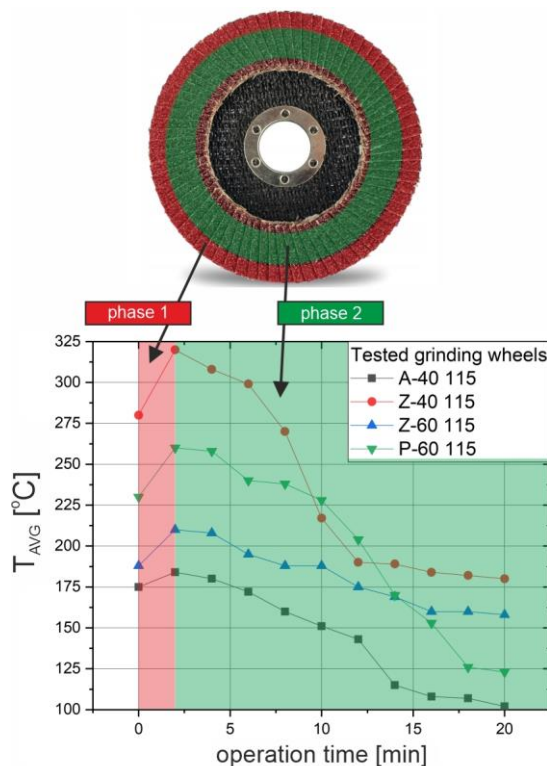


Fig. 14. Experimentally determined dependences of the temperature T_{AVG} on the operating time of the grinding wheels.

5. CONCLUSIONS

1. The tests were carried out on a population of 1050 manufactured flap discs in 32 generic groups described by the codes types: PL29 115X2.5 3 1 2, PL29 115X4.0 4B 1 2, PL29 115X4.0 4B 2 2 and

PL29 115X4.0 4A 1 2. As a result of the research, the limit values of the parameters for the construction and operation of the tested abrasive tools were obtained.

2. The final result of the study is a set of analytical

models of factors important for the construction of the flap discs and their effective and safe operation, i.e. models of background wear as a function of the percentage of filler content (2), the burst resistance of the background of the disc (3), the adhesive connection of the pad with the background (4), and the limit speed of the pad and granulation of the abrasive flaps (5).

3. The results of the calculations led to the creation the general functional models and to develop a technology for the production of new types of abrasive tools with a similar structure and method of operation.
4. On the basis of the results obtained from the main tests, it can be concluded that higher values of the maximum average contact temperature were obtained for new grinding wheels. In addition, the higher temperature value was influenced by higher loads on the grinding wheels.
5. The highest temperature values for each grinding wheel were determined for test 7 according to the test plan (new grinding wheel, load 3 kg, working angle

of the grinding wheel 20°). The lowest temperature values for each grinding wheel were determined for test no 2 (worn grinding wheel, load 1 kg, working angle of the grinding wheel 2°). The highest contact temperature values were determined during operation with the Z-40 grinding wheel. For test number 7, the value of temperature was $T_{AVG} = 450$ °C, while for test number 2, the value of temperature was $T_{AVG} = 80$ °C.

Suggestions for further work

- It is suggested to widen the research to machining of other materials, including the titanium-based hard-to-cut materials.
- In addition, it is planned to perform the research for various machined materials, which will allow determining new ranges of machining parameters, taking into account the grinding wheel wear rate.
- The expansion of the test stand to include the measurement of forces during the grinding process by means of using a 3-axis piezoelectric dynamometer.

Reference

1. Adibi H, Rezaei Ahmed S M, Sarhan A D. Analytical modeling of grinding wheel loading phenomena. *International Journal of Advanced Manufacturing Technology* 2013; 68: 473-485, <https://doi.org/10.1007/s00170-013-4745-z>.
2. Arriandiaga A; Portillo E; Sánchez J A; Cabanes I; Pombo I. Virtual Sensors for On-line Wheel Wear and Part Roughness Measurement in the Grinding Process. *Sensors* 2014, 14, 8756-8778. <https://doi.org/10.3390/s140508756>.
3. Axinte D, Butler-Smith P, Akgun C, Kolluru K. On the influence of single grit microgeometry on grinding behavior of ductile and brittle materials. *International Journal of Machine Tools and Manufacture* 2013; 74: 12-18, <https://doi.org/10.1016/j.ijmachtools.2013.06.002>.
4. Borucka A, Kozłowski E, Parczewski R, Antosz K, Gil L, Pieniak D. Supply Sequence Modelling Using Hidden Markov Models. *Applied Sciences*. 2023; 13(1):231. <https://doi.org/10.3390/app13010231>
5. Demko, M.; Vrabel, M.; Maňková, I.; Ižol, P. Cutting tool monitoring while drilling using internal CNC data. *Procedia CIRP* 2022, 112, 263–267. <https://doi.org/10.1016/j.procir.2022.09.082>.
6. Guo G; Malkin S. *Grinding Technology Theory and Applications of Machining with Abrasives*, 2nd ed.; Industrial Press: New York, NY, USA, 2008; pp. 257–270.
7. Herzenstiel P, Aurich J C. CBN-grinding wheel with a defined grain pattern -extensive numerical and experimental studies, *Machining Science and Technology* 2010; 14: 301-322, <https://doi.org/10.1080/10910344.2010.511574>.
8. Jackson M J, Mills B. Microscale wear of vitrified abrasive materials. *Journal of Materials Science* 2004; 39: 2131-2143, <https://doi.org/10.1023/B:JMSE.0000017776.67999.86>.
9. Kacalak W, Lipiński D, Rypina Ł, Szafraniec F, Tandecka K, Bałasz B. Performance evaluation of the grinding wheel with aggregates of grains in grinding of Ti-6Al-4V titanium alloy. *International Journal of Advanced Manufacturing Technology* 2018; 94: 301-314, <https://doi.org/10.1007/s00170-017-0905-x>.
10. Kacalak W, Lipiński D, Szafraniec F, Banaszek K, Rypina Ł. Probabilistic Aspects of Modeling and Analysis of Grinding Wheel Wear.

Materials 2022, 15, 5920. <https://doi.org/10.3390/ma15175920>.

11. Karabacak Y. E, Deep learning-based CNC milling tool wear stage estimation with multi-signal analysis, *Eksplotacja i Niezawodność – Maintenance and Reliability* 2023; 25(3) <http://doi.org/10.17531/ein/168082>
12. Katalog materiałów ściernych. Koło: Andre Abrasives, 2017.
13. Kato T, Fuji H. Temperature measurement of workpieces in conventional surface grinding. *Journal of Manufacturing Science and Engineering* 2000; 122: 297-303, <https://doi.org/10.1115/1.538918>.
14. Kawa P, Świdorski A, Wybrane narzędzia statystyczne w zastosowaniu do oceny jakości wyrobów. *Gospodarka Materialowa & Logistyka* 2016, nr 10/2016.
15. Kopytowski A, Świercz R, Oniszczuk-Świercz D, Zawora J, Kuczak J, Źrodowski Ł. Effects of a New Type of Grinding Wheel with Multi-Granular Abrasive Grains on Surface Topography Properties after Grinding of Inconel 625. *Materials* 2023, 16, 716. <https://doi.org/10.3390/ma16020716>.
16. Kozłowski E, Borucka A, Oleszczuk P, Jałowiec T. Evaluation of the maintenance system readiness using the semi-Markov model taking into account hidden factors. *Eksplotacja i Niezawodność – Maintenance and Reliability*. 2023;25(4). <https://doi.org/10.17531/ein/172857>
17. Kumar, S.S., Uthayakumar, M., Kumaran, S.T. et al. Performance Monitoring of WEDM Using Online Acoustic Emission Technique. *Silicon* 10, 2635–2642 (2018). <https://doi.org/10.1007/s12633-018-9800-9>
18. Marinescu I D, Hitchiner M, Uhlmann E, Rowe W B. Inasaki I.. *Handbook of Machining with Grinding Wheels*. CRC Press, Boca Raton, 2007. <https://doi.org/10.1201/9781420017649>
19. Malkin S, Guo C. Thermal analysis of grinding. *Annals of the CIRP* 2007; 56: 760 - 782, <https://doi.org/10.1016/j.cirp.2007.10.005>.
20. Mgherony, A., Mikó, B. The effect of the spindle speed control when milling free-form surfaces. *Int J Adv Manuf Technol* (2023). <https://doi.org/10.1007/s00170-023-12811-1>
21. Nadolny K. Wear phenomena of grinding wheels with sol-gel alumina abrasive grains and glass-ceramic vitrified bond during internal cylindrical traverse grinding of 100Cr6 steel. *International Journal of Advanced Manufacturing Technology* 2015; 77: 83-98, <https://doi.org/10.1007/s00170-014-6432-0>.
22. Nosenko V A, Fedotov E V, Nosenko S V et al. Probabilities of abrasive tool grain wearing during grinding. *J. Mach. Manuf. Reliab.* 38, 270–276 (2009). <https://doi.org/10.3103/S1052618809030108>.
23. Persson B N J, 2006. Contact mechanics for randomly rough surfaces. *Surf. Sci. Rep.* 61 (4), 201–227. doi:10.1016/j.surfrep.2006.04.001.
24. Rasim M, Mattfeld P, Klocke F. Analysis of the grain shape influence on the chip formation in grinding. *Journal of Materials Processing Technology* 2015; 226: 60-68, <https://doi.org/10.1016/j.jmatprotec.2015.06.041>.
25. Salonitis K, Chondros T, & Chryssolouris G. Grinding wheel effect in the grind-hardening process. *Int J Adv Manuf Technol* 38, 48–58 (2008). <https://doi.org/10.1007/s00170-007-1078-9>.
26. Scherge M, Martin J M, Pöhlmann K. Characterization of wear debris of systems operated under low wear-rate conditions. *Wear* 2006; 260 (4), 458–461. doi:10.1016/j.wear.2005.03.025.
27. Souza A M, da Silva E J, Global strategy of grinding wheel performance evaluation applied to grinding of superalloys, *Precision Engineering*, Volume 57,2019,Pages 113-126,ISSN 0141-6359, <https://doi.org/10.1016/j.precisioneng.2019.03.013>.
28. Sun Y, Vu T T, Halil, Z.; Yeo, S.H.; Wee, A. Material removal prediction for contact wheels based on a dynamic pressure sensor. *Int. J. Adv. Manuf. Technol.* 2017; 93, 945–951. <https://doi.org/10.1007/s00170-017-0473-0>
29. Talon A G, Sato B K, Rodrigues Md. et al. Green manufacturing concept applied to the grinding process of advanced ceramics using an alternative lubri-refrigeration technique. *Int J Adv Manuf Technol* 2022; 123, 2771–2782. <https://doi.org/10.1007/s00170-022-10385-y>.
30. Tönshoff K H, Friemuth T, Becker J C. Process monitoring in grinding. *Annals of the CIRP*, 2002; 51: 551-571, [https://doi.org/10.1016/S0007-8506\(07\)61700-4](https://doi.org/10.1016/S0007-8506(07)61700-4).
31. Uhlmann E, Lypovka P, Hochschild L, Schröer N. Influence of rail grinding process parameters on rail surface roughness and surface layer hardness. *Wear* 2016; 366-367:287-293, <https://doi.org/10.1016/j.wear.2016.03.023>.
32. Ullah A S, Caggiano A, Kubo A, Chowdhury M A K. Elucidating Grinding Mechanism by Theoretical and Experimental Investigations.

Materials 2018; 11, 274. <https://doi.org/10.3390/ma11020274>.

33. Wang H, Zhang Z, Li J, Xin W, Han C, Fault analysis and reliability evaluation for motorized spindle of cycloidal gear grinding machine based on multi-source bayes, *Eksploatacja i Niezawodność – Maintenance and Reliability* 2024; 26(1)<http://doi.org/10.17531/ein/175010>
34. Wang J, Liu X, Wang X, Jin K, Process machining allowance for reliability analysis of mechanical parts based on hidden quality loss, *Eksploatacja i Niezawodność – Maintenance and Reliability* 2023; 25(4) <http://doi.org/10.17531/ein/171594>
35. Wang S, Li C. Application and development of high-efficiency abrasive process. *Int. J. Adv. Sci. Technol.* 2012; 47, 51–64.
36. Wegener K, Hoffmeister W, Karpuschewski B, Kuster F, Hahmann W C, Rabiey M. Conditioning and monitoring of grinding wheels. *CIRPAnnals* 2011; 60: 757-777, <https://doi.org/10.1016/j.cirp.2011.05.003>.